Phase transitions and iron-ordered moment form factor in LaFeAsO

H.-F. Li,[1,*] W. Tian,[1] J.-Q. Yan,[1] J. L. Zarestky,[1] R. W. McCallum,[1,2] T. A. Lograsso,[1] and D. Vaknin[1,3,†]
[1]*Ames Laboratory, US-DOE, Ames, Iowa 50011, USA*
[2]*Department of Materials Science and Engineering, Iowa State University, Ames, Iowa 50011, USA*
[3]*Department of Physics and Astronomy, Iowa State University, Ames, Iowa 50011, USA*
(Received 21 June 2010; revised manuscript received 12 July 2010; published 9 August 2010)

Elastic neutron-scattering studies of single-crystal LaFeAsO reveal that upon cooling, an onset of the tetragonal (T)-to-orthorhombic (O) structural transition occurs at $T_S \approx 156$ K, and it exhibits a sharp transition at $T_P \approx 148$ K. We argue that in the temperature range T_S to T_P, T and O structures may dynamically coexist possibly due to nematic spin correlations recently proposed for the iron pnictides, and we attribute T_P to the formation of long-range O domains from the finite local precursors. The antiferromagnetic structure emerges at $T_N \approx 140$ K, with the iron moment direction along the O *a* axis. We extract the iron magnetic form factor and use the tabulated $\langle j_0 \rangle$ of Fe, Fe^{2+}, and Fe^{3+} to obtain a magnetic moment size of ~ 0.8 μ_B at 9.5 K.

DOI: 10.1103/PhysRevB.82.064409 PACS number(s): 74.25.Ha, 74.70.Xa, 75.30.Fv, 75.50.Ee

I. INTRODUCTION

The discovery of $R\mathrm{FeAs}(O_{1-x}F_x)$ (R=rare earth, "1111") superconductors[1] with transition temperatures up to 56 K (Refs. 2 and 3) has stimulated a renewed excitement in the search for novel superconductors derived from antiferromagnetic (AFM) parent compounds. In these iron-arsenide-based compounds, the superconducting (SC) state can be achieved by doping or by the application of pressure. The appearance of superconductivity is normally accompanied by a suppression of the AFM state in the parent compounds and by the appearance of a spin resonance.[4,5] It is thus important to understand the magnetism in these iron-based parent compounds in order to unravel the mechanism that leads to superconductivity.

Because of the initial difficulties to grow large 1111 single crystals, most of the research on these systems has been performed on polycrystalline samples. These studies showed that LaFeAsO undergoes a structural phase transition from the tetragonal (T, $P4/nmm$) symmetry [Fig. 1(a)] to the orthorhombic (O, *Cmma*) one [Fig. 1(b)] at $T_S \approx 155$ K and forms an AFM ordering (also referred to as a spin-density wave) at $T_N \approx 137$ K upon cooling, with an ordered magnetic moment of 0.36(5) μ_B.[6] Implied in these reports on powdered polycrystalline samples[6–8] is that the form factor used is that of Fe^{2+} ion. However, first-principles calculations on LaFeAsO predict a larger localized magnetic moment of ~ 2.6 μ_B at each iron site that is embedded in an itinerant electronic environment.[9] It should be noted that density-functional theory argues that a large enough magnetic moment ~ 2 μ_B is necessary to drive the observed orthorhombic-tetragonal (O-T) transition.[10] It is clear that there is a significant discrepancy between the calculated iron moment and the experimental one. Therefore, determining the moment size is vital to the validity of any theoretical model that attempts to explain the electronic structure of LaFeAsO. Another important issue is the coupling between structural and magnetic behaviors in iron pnictides. Inelastic neutron-scattering studies from polycrstalline LaFeAsO showed two-dimensional (2D) magnetic fluctuations that persist up to room temperature (over ~ 160 K above T_N). It was argued[11–13] that such fluctuations introduce dynamic disorder of the O/T mixed phase in the so-called T phase, suggesting that a finite orthorhombicity may exist above the O-T structural transition.[11–13]

The polycrystalline studies have provided important insights into the behavior of LaFeAsO but questions remain with regard to the AFM moment direction, the moment size and its spatial distribution. To a large extent, these questions are related to the complexity of iron chemistry, namely, its valence (or mixed-valence), bonding, and electron configuration in different local chemical surroundings. To address these questions, the study of high-quality single crystals is vital. Such crystals are now available with the recent successful growth of relatively large 1111 single crystals at ambient pressure.[14]

Here we report elastic neutron-scattering and synchrotron x-ray powder-diffraction studies on the bulk and pulverized LaFeAsO single crystals, respectively, focusing on the de-

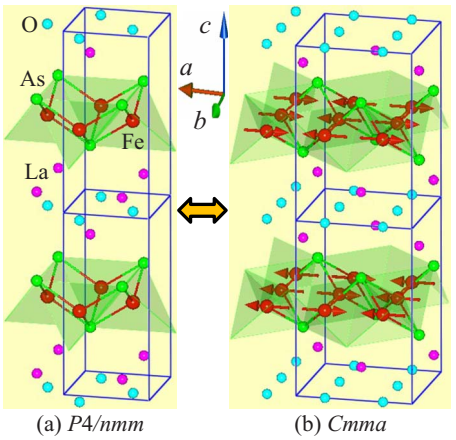

(a) *P4/nmm* (b) *Cmma*

FIG. 1. (Color online) (a) Crystal structure ($P4/nmm$) above $T_S = 156(1)$ K with two unit cells (solid lines). (b) Crystal structure (*Cmma*) below T_S with two unit cells (solid lines) and AFM structure below $T_N = 140(1)$ K in one AFM unit cell. The arrows on the Fe ions in (b) represent the spins of iron in single-crystal LaFeAsO. The unit cells of $P4/nmm$ (T), *Cmma* (O) and AFM structures are (a b c) ($a = b$), ($\sqrt{2}a$ $\sqrt{2}b$ c) and ($\sqrt{2}a$ $\sqrt{2}b$ $2c$), respectively.

tails of the structural and magnetic transitions as well as the coupling between them, and the measurement of the average ordered magnetic moment size and its spatial distribution by extracting the magnetic form factor of iron in this compound.

II. EXPERIMENTAL

LaFeAsO single crystals were synthesized in an NaAs flux at ambient pressure as described in a recent report.[14] Crystal quality was characterized by Laue backscattering, x-ray powder-diffraction, heat-capacity, magnetization, and resistivity measurements. A large LaFeAsO single crystal (~20 mg) was selected for this study. The mosaic of this single crystal is 0.59(2)° full width at half maximum (FWHM) for the $(202)_O$ (O notation) reflection at room temperature. The elastic neutron-scattering measurements were carried out on the HB-1A fixed-incident-energy (14.6 meV) triple-axis spectrometer using a double pyrolytic graphite (PG) monochromator (located at the high flux isotope reactor, HFIR, at the Oak Ridge National Laboratory, USA). Two highly oriented PG filters, one after each monochromator, were used to reduce the $\lambda/2$ contamination. The beam collimation throughout the experiment was kept at 48′-48′-sample-60′-360′. The single crystal was wrapped in Al foil and sealed in a He-filled Al can which was then loaded on the cold tip of a closed cycle refrigerator with $(h0l)_O$ in the *Cmma* symmetry as the scattering plane. The synchrotron x-ray powder-diffraction study of pulverized LaFeAsO single crystals from the same batch as the one used for the neutron-diffraction study was carried out at the 11-BM beamline, Advanced Photon Source, Argonne National Laboratory. 11-BM is a bending magnet beamline, equipped with a vertical beam collimation mirror, a double crystal monochromator with a horizontal sagittal focusing second crystal, and a vertical focusing mirror. The calibrated x-ray wavelength was 0.41219(1) Å. We note that the $(HKL)_T$ indices for T symmetry correspond to the O reflection $(hkl)_O$ based on the relations $h=H+K$, $k=H-K$, and $l=L$.

III. RESULTS AND DISCUSSION

A. Structural and magnetic transitions

A room-temperature x-ray powder-diffraction pattern of pulverized LaFeAsO single crystals from the same batch as the one used in this study measured on an in-house diffractometer is shown in Fig. 2 (dots), where the best structure refinement with $P4/nmm$ symmetry using FULLPROF suite[15] is also displayed (solid line), yielding a good fit ($\chi^2=1.18$) and indicating a high degree of phase purity of the single crystals. The refined structural parameters listed in Table I are in agreement with previous reports.[7,14]

Figure 3 shows the temperature evolution of the structural and magnetic transitions in the single crystal measured by neutron diffraction on HB-1A. For the structural transition, the $(400)_O/(040)_O$ and $(006)_O$ (*Cmma*) reflections were monitored. The integrated intensity of the rocking-curve scans of the $(400)_O$ reflection shows an appreciable increase at ~156 K, with a relatively sharp maximum at ~148 K.

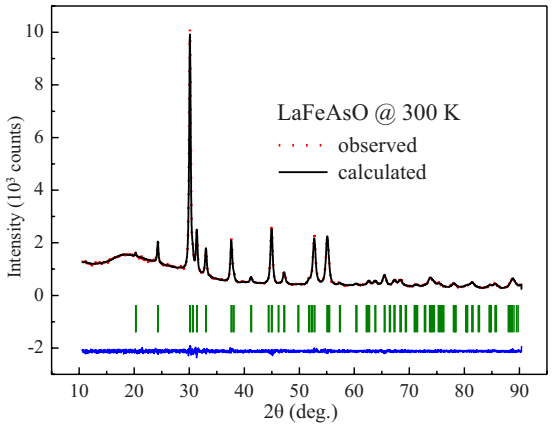

FIG. 2. (Color online) Observed (dots) and calculated (solid line) x-ray powder-diffraction patterns for pulverized LaFeAsO single crystals at ambient conditions obtained on an in-house diffractometer employing the copper $K_{\alpha1}=1.54056$ Å and $K_{\alpha2}=1.54439$ Å with $I_{\alpha2}/I_{\alpha1}=0.5$ as the radiation. The vertical bars mark the positions of Bragg reflections. The lower curve represents the difference between the observed and calculated patterns.

The scattering at the $(400)_O/(040)_O$ rocking curves or θ-2θ scans is strongly influenced by twinning formation upon cooling[13] that may increase the in-plane mosaicity in the crystal due to nucleation of domains with different orientations at different sites. Based on these observations, we suggest two critical temperatures for the structural transition: first, at $T_S \sim 156$ K, the finite local O domains begin to form side by side with major T domains in a slightly disordered manner; second, at $T_P \sim 148$ K, the local O precursors have grown into long-range O domains. The temperature range between T_S and T_P may be considered as a coexisting regime of the T and O phases. The splitting of the $(HKL)_T$ ($P4/nmm$) reflection into twinned $(H+K,H-K,L)/(H-K,H+K,L)$ (*Cmma*) reflections is a sensitive measure of the T-to-O structural transition. To track the O splitting, we performed a high-resolution synchrotron x-ray powder-diffraction study with pulverized LaFeAsO single crystals. Part of the data is displayed in Fig. 4 which clearly shows the splitting of $(220)_T$ to $(400)_O/(040)_O$ and $(322)_T$ to $(512)_O/(152)_O$ at 130 K below the O-T transition. It is noted that the $(220)_T$ reflection at 158 K is broader than the $(400)_O$ reflection at 130 K. This may indicate a distribution of d spacings due to O-T fluctuations above T_S. In

TABLE I. Refined structural parameters with T ($P4/nmm$) symmetry for pulverized LaFeAsO single crystals at room temperature. $a=4.0316(1)$ Å, $c=8.7541(1)$ Å, $V=142.290(1)$ Å^3, $R_B=1.01$, $R_F=0.60$, and $\chi^2=1.18$.

Atom	Site	x	y	z	B (Å^2)
La	2*c*	0.25	0.25	0.1405(2)	1.65(4)
Fe	2*b*	0.75	0.25	0.5	1.69(12)
As	2*c*	0.25	0.25	0.6543(3)	2.15(8)
O	2*a*	0.75	0.25	0.0	Insensitive

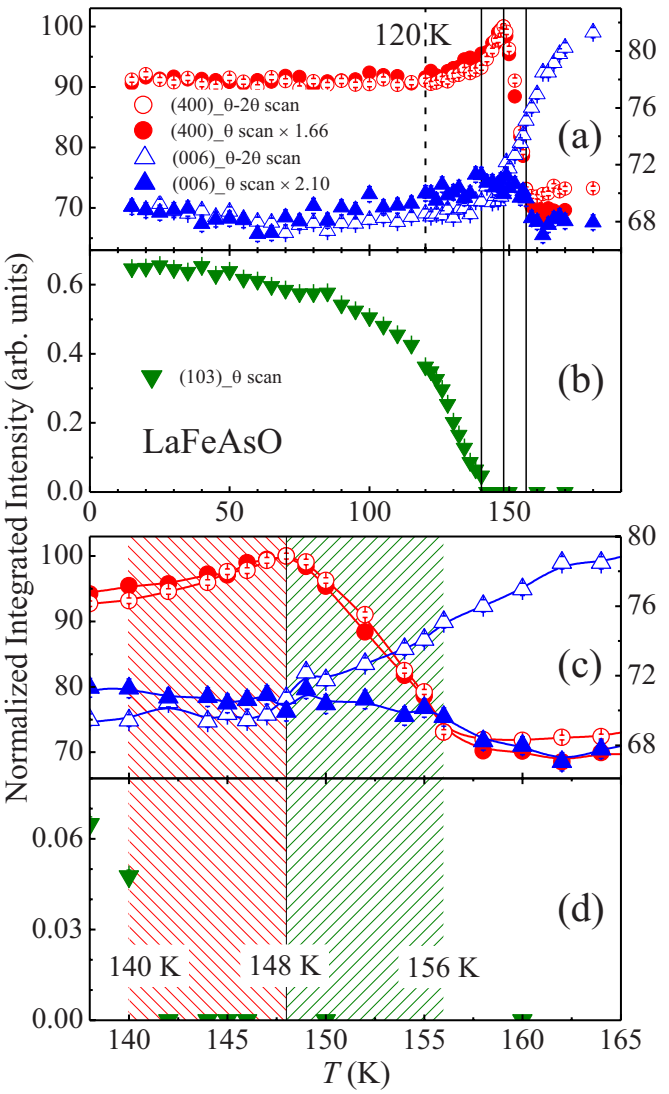

FIG. 3. (Color online) Temperature dependence of the normalized integrated intensities of (a) θ-2θ (void symbols) and rocking-curve θ (solid symbols) neutron-diffraction scans of the nuclear Bragg $(400)_O$ (circles) and $(006)_O$ (triangles) reflections, and (b) the neutron rocking-curve scan of the AFM (103) reflection (down-solid-triangles) of single-crystal LaFeAsO measured upon warming up the crystal from 9.5 K. (c) and (d) are the enlargements of (a) and (b) near the structural and AFM transitions, respectively. The integrated intensities of $(400)_O$ and $(006)_O$ rocking curves are rescaled by 1.66 and 2.10, respectively, as indicated to make them coincide with the respective θ-2θ scans at low temperatures.

Fig. 5, we show the temperature variation in the FWHM of the $(004)_{O/T}$ and $(220)_T$ reflections obtained from a Lorentzian fit function to the Bragg peaks shown in Fig. 4. While the width variation in the $(004)_{O/T}$ reflection is negligible within errors, the variation in the $(220)_T$ reflection is more significant showing a maximum at ~150 K. The normalized FWHM of the $(220)_T$ reflection to that of the $(004)_{O/T}$ reflection displays an asymmetric temperature variation with a larger FWHM above the O-T transition [Fig. 5(b)]. This indicates a remnant orthorhombicity at temperatures as high as 300 K. This is consistent with Ref. 12 where a finite orthorhombicity remains visible above T_P up to 200 K. Similar

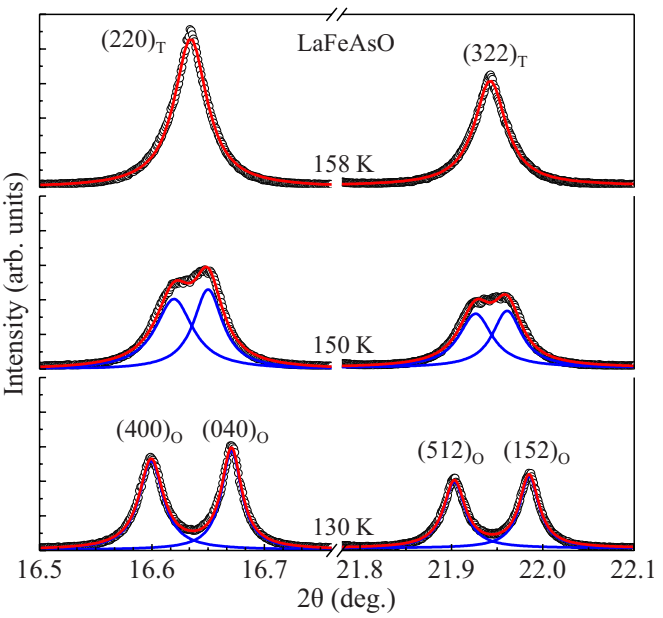

FIG. 4. (Color online) Synchrotron x-ray powder-diffraction data of pulverized LaFeAsO single crystals above (158 K), during (150 K) and below (130 K) the O-T transition (circles). The solid lines are fits of the Lorentzian line shape.

observations have also been found in $SrFe_2As_2$.[11,13] We thus argue that both T and O phases may coexist dynamically due to the strong magnetic correlations in a certain temperature range[12] above T_N, which can be ascribed to a spin nematic phase.[16–18] We, therefore, associate T_P=148(1) K as the O-T phase transition temperature in the single-crystal LaFeAsO. We argue that this transition temperature (T_P) may vary slightly, depending on the sample quality,[18] size, and shape, and the cooling/warming protocols.

Figures 3(b) and 3(d) show the temperature dependence of the rocking-curve integrated intensity of the AFM (103) reflection. The magnetic peak appears at ~140 K, indicating the formation of the AFM structure as shown in Fig. 1(b).

B. Magnetic form factor of iron

To obtain the magnetic form factor of iron in LaFeAsO, we collected the integrated intensities of the rocking curves of nuclear and magnetic Bragg reflections to the highest-order possible with the HB-1A spectrometer. The nuclear reflections, necessary to obtain the magnetic moment size, were chosen to be able to cover as much of the q range of the measured AFM reflections as possible. This reduces any errors due to geometry corrections, Debye-Waller factor (DWF), absorption effects, and others. The integrated intensity of the rocking curve of a nuclear Bragg reflection at a reciprocal lattice vector $\mathbf{q}$ in a crystal is given by

$$I_N = \frac{V}{v_0^2}\Phi_0(\theta)|F_N(\mathbf{q})|^2\frac{\lambda^3}{2\mu\sin(2\theta)}e^{-2W}$$

$$= \frac{C_N(\mathbf{q})|F_N(\mathbf{q})|^2}{\sin(2\theta)}, \quad (1)$$

where V is the scattering volume of the crystal, v_0 is the unit-cell volume, $\Phi_0(\theta)$ is the beam flux at the angle θ,

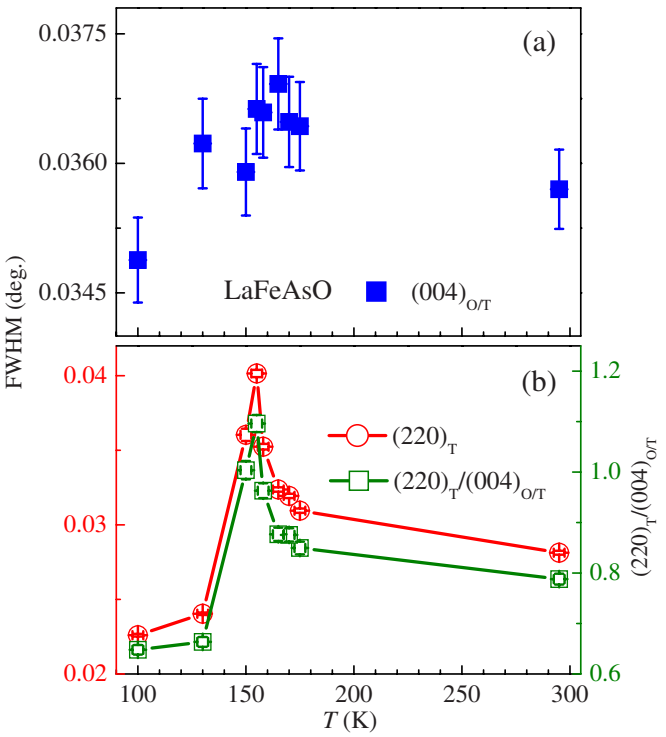

FIG. 5. (Color online) Temperature variation in FWHM of the $(004)_{O/T}$ (a) and $(220)_T$ (circles) (b) reflections from synchrotron x-ray powder-diffraction study of pulverized LaFeAsO single crystals. Below the O-T structural transition, the FWHM of the $(220)_T$ reflection was averaged from the $(400)_O$ and $(040)_O$ reflections. To avoid the influence of systematic errors, we normalized the FWHM of the $(220)_T$ reflection to that of the $(004)_{O/T}$ shown as squares in (b). The lines in (b) are guides to the eye.

$F_N(\mathbf{q})$ is the structure factor, λ is the beam wavelength, μ is the absorption length, $\sin(2\theta)$ is the Lorentz factor for a rotating crystal, and $2W=\mathbf{q}^2\langle u_Q\rangle^2$ is the DWF. We collect all the constants and unknown $\mathbf{q}$-dependent factors in $C_N(q)$, including the DWF. The integrated intensities of the rocking curves of the chosen nuclear Bragg reflections were normalized to the corresponding structure factors and the Lorentz factors. The data were also corrected for the fact that the rocking curve of nuclear Bragg peaks in our measurements includes an equivalent twinned $(h00)$ and $(0k0)$ domains,[19] for normalization of the magnetic reflections which are due to the $(h00)$ domain only. The results are shown in Fig. 6(a) (circles). We assume $C_N(q)$ is a DWF-like function (namely, a Gaussian) and fit the data by the nonlinear square technique to obtain a smooth $C_N(q)$ function shown as a solid line in Fig. 6(a).

Similarly, the scattered intensity of the rocking curve of a magnetic Bragg reflection can be expressed as

$$I_M = C_M(\mathbf{q})\left(\gamma_n r_e \frac{1}{2} gS\right)^2 f_M^2(|\mathbf{q}|)|F_M(hkl)|^2 \sin^2\alpha \frac{1}{\sin(2\theta)}, \quad (2)$$

where $C_M(\mathbf{q})=C_N(\mathbf{q})/4$ due to the fact that the AFM unit cell is doubled along the crystallographic c axis in comparison with the nuclear one [Fig. 1(b)], $\gamma_n=-1.913$,

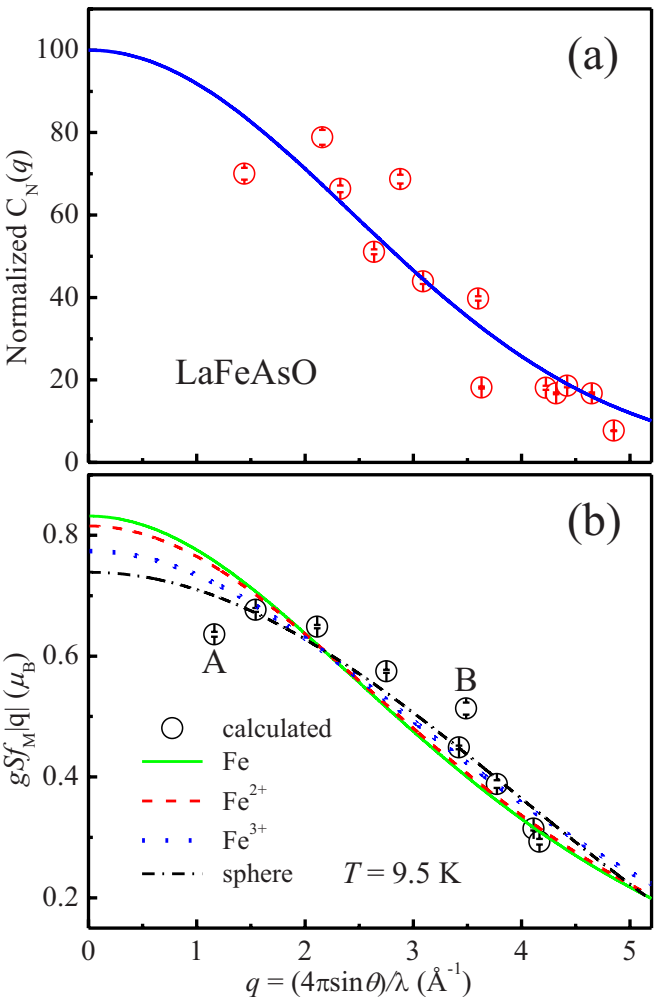

FIG. 6. (Color online) (a) q dependence of the collected factor $C_N(q)$ (circles) in Eq. (2) at 9.5 K as described in the text. The nuclear Bragg reflections were chosen to cover the q range of the measured AFM reflections as possible. The intensities of nuclear reflections were integrated from their respective rocking curves, taking into account the domain effect, and normalized to the corresponding structure factors and the Lorentz factors. The collected factor $C_N(q)$ contains the DWF and other effects such as extinctions and absorption. The solid line is the best DWF-like curve that best fits the data and is used to normalize the AFM peaks to obtain the magnetic form factor of iron in single-crystal LaFeAsO. (b) Measured magnetic form factor of iron (circles) at the AFM phase (9.5 K) of single-crystal LaFeAsO. The lines as indicated are the best fits of the data with the magnetic moment $M(\mu_B)$ multiplied by the calculated form factors $\langle j_0\rangle$ of Fe, Fe^{2+} and Fe^{3+} with spin contribution only (Ref. 20), and the form factor of a homogeneous sphere (details in text), respectively. The fitted results are shown in Table III. The deviation of A and B points from the smooth curves is discussed in the text.

$r_e=2.81794\times10^{-5}$ Å is the classical electron radius, $f_M(|\mathbf{q}|)$ is the magnetic form factor at the magnetic reciprocal lattice $(\mathbf{q})$, $|F_M(hkl)|=|\Sigma e^{2\pi i(hx_j+ky_j+lz_j)}|=8$ $(j=1-8)$ where $(x_j\ y_j\ z_j)$ represents fractional coordinates of the jth atom in the AFM unit cell, and $\sin^2\alpha=1-(\hat{\mathbf{q}}\cdot\hat{\mu})^2$, where $\hat{\mathbf{q}}$ and $\hat{\mu}$ are the unit vectors along the scattering vector and the direction of the moment, respectively. Our attempt to calculate the

TABLE II. The q values, integrated intensities, and the corresponding values of $|F_M(hkl)|^2\sin^2\alpha$ at 9.5 K of the AFM reflections observed in single-crystal LaFeAsO with the AFM structure as shown in Fig. 1(b).

$(h0l)$	q (Å^{-1})	Intensity	$\lvert F_M(hkl)\rvert^2\sin^2\alpha$
(101)	1.162	26.55 ± 0.35	6.138
(103)	1.545	107.50 ± 1.00	31.251
(105)	2.111	94.08 ± 0.81	46.470
(107)	2.751	53.87 ± 0.48	53.670
(109)	3.422	22.21 ± 0.31	57.325
(303)	3.487	2.98 ± 0.11	6.138
(305)	3.773	3.35 ± 0.11	14.560
(1011)	4.110	7.29 ± 0.13	59.373
(307)	4.164	2.42 ± 0.08	23.424

magnetic form factor with various directions of the ordered magnetic moment yielded an irregular and unphysical form factor, except when the moment points along the O a axis, namely, $\hat{\mu}=(100)$. This is strong confirmation that the AFM moment direction is along the O a axis. In Table II, we list all the observed magnetic reflections, their integrated intensities, and the corresponding values of $|F_M(hkl)|^2\sin^2\alpha$. Using these parameters and Eq. (2), we calculated the value of $gSf_M(|\mathbf{q}|)$ as shown in Fig. 6(b) (circles). To obtain the behavior of the form factor, we fit the data in Fig. 6(b) to different model form factors of iron in different environments. In general, we find that the form factor behavior is very similar to the one recently measured and calculated for $SrFe_2As_2$.[21] Fitting the data with the theoretical form factors of Fe, Fe^{2+}, and Fe^{3+} ($\langle j_0\rangle$, spin contribution only) in Ref. 20, we obtain the corresponding average AFM moment sizes $M(\mu_B)$ as listed in Table III. The experimental points indicated as A and B in Fig. 6(b) deviate from the smooth curves, which may be due to systematic errors or due to some subtle features of the magnetic structure and its dynamics that are not captured by our structure factor determination.

As a simple, heuristic model, we assume that the magnetic moment is homogeneously distributed within a sphere of radius R, for which the form factor can be simply calculated by $f(q)=3\frac{\sin(qR)-qR\cos(qR)}{(qR)^3}$. Fitting our measured data [circles in Fig. 6(b)] with this equation yields an average moment size of $(0.74\pm0.04)\ \mu_B$ with a radius $R=(0.63\pm0.04)$ Å. This radius is almost the same as the effective ionic radius of Fe^{2+}(0.63 Å) (Ref. 22) with a coordination number of 4, suggesting that the oxidation state of iron in LaFeAsO is closer to that of Fe^{2+}. It is pointed out that the effective ionic radius depends on the particular electron configuration as well as the surrounding ions (As) and the relative amount of ionic bonding.

TABLE III. The fitted results of Fig. 6 with different form factors $\langle j_0\rangle$ of Fe, Fe^{2+} and Fe^{3+} with spin contribution only (Ref. 20), and a homogeneous spherical model (details in text): the corresponding magnetic moment size M (μ_B) and ionic radius R (Å). The effective ionic radius of Fe^{2+} and Fe^{3+} was taken from Ref. 22 with the CN=4.

Models	M (μ_B)	R (Å)
$SrFe_2As_2$/bcc iron	0.83 ± 0.04	
Fe^{2+}	0.82 ± 0.03	0.63
Fe^{3+}	0.77 ± 0.03	0.49
Sphere	0.74 ± 0.04	0.63 ± 0.04

The average magnetic moment is ~0.8 μ_B in the AFM phase of single-crystal LaFeAsO in disagreement with the reported smaller value of ~0.37 μ_B (polycrystal)[6] but more or less near the recently reported ~0.63(1) μ_B (polycrystal).[12] In addition, the obtained moment size in this study is almost the same as the first-principles-optimized 0.87 μ_B in the magnetically frustrated state,[23] the ~0.83 μ_B in an oxygen-deficient LaFeAsO (polycrystal),[24] and the ~0.8 μ_B in CeFeAsO (polycrystal).[25] First, it is pointed out that there is a large difference in the properties of polycrystalline and single-crystalline samples, especially for those containing easily sublimating elements or oxides, e.g., the nominal $La_{0.875}Sr_{0.125}MnO_3$.[26–28] Second, single crystals are believed to be more stoichiometric[26,28] and maintain translational symmetry over macroscopic distances, in contrast with polycrystals, thereby providing more reliable information on the structures and intrinsic properties. The small magnetic moment size ~0.8 μ_B (compared to Fe^{2+} in an insulator, $S=2$ with an average ordered localized moment 4 μ_B) is comparable to that of the AFe_2As_2 (A=Ca, Sr, Ba, 122) suggesting an effective $S\approx\frac{1}{2}$ on the iron sites,[21] and to some extent points to the itinerant character of the magnetism in this system. This puts the 1111 compound on a similar par with the other "122" parent compounds with a magnetic moment that is in the range of 0.8–1.1 μ_B. This suggests a sharp jump in the magnetic moment of Fe ions as a function of the Fe-As distance to about 1 μ_B, as predicted from first-principles calculations of bulk zinc-blende FeAs.[29]

There are a few possible explanations to the small magnetic moment measured by neutron-diffraction techniques in iron pnictides. The most accepted one is that it is due to the itinerant character of magnetism in this system. On the other hand, in a local moment picture this may be due to the dimensionality of the system or due to competing nearest-neighbors (NNs) and next-NN (NNN) exchange interactions. The Fe layers are weakly coupled making each layer behave as a quasi-2D system. The 2D systems, especially those with isotropic NN coupling, exhibit strong magnetic fluctuations that can lower the quasi-static ordered magnetic moment. Second, the unusual spin arrangement observed in iron pnictides indicates the presence of strong competing and conflicting interactions between NN (J_1) and NNN (J_2) that can lead to strong magnetic fluctuations and a reduced static moment.

To summarize, employing both neutron- and synchrotron diffraction techniques to explore the details of the structural and magnetic properties of single-crystal LaFeAsO, we found: (1) the O-T structural transition occurs at $T_P\approx148$ K but the finite local O precursors appear to form already at $T_S\approx156$ K. We argue that the T and O phases may coexist in the temperature range of T_S and T_P, and at T_P the long-range O phase has formed. (2) The AFM structure

forms at $T_N \approx 140$ K upon cooling with the iron moment direction along the crystallographic a axis in the O phase. (3) The average AFM moment size is comparable to that of the AFe_2As_2 (A=Ca, Sr, Ba), e.g., $M=(0.82\pm0.03)$ μ_B with a form factor of Fe^{2+} with spin contribution only. This moment size is significantly larger than the previously reported values. More detailed studies of the form factor will be required to determine the possibility of the recently predicted spin spatial anisotropy.[21] This study shows that to a large extent the properties of LaFeAsO are very similar to those of the so-called 122 systems.

ACKNOWLEDGMENTS

D.V. wishes to thank R. J. McQueeney for the many illuminating discussions on the properties of FeAs-based compounds. J.-Q.Y., R.W.M., and T.A.L. thank B. Jensen and K. W. Dennis for their help in crystal growth and characterization. The authors thank Matthew Suchomel for running the powder diffraction measurements on 11-BM on the x-ray Operations and Research Beamline 11-BM at the Advanced Photon Source, Argonne National Laboratory. Research at Ames Laboratory is supported by the U.S. Department of Energy, Office of Basic Energy Sciences, Division of Materials Sciences and Engineering under Contract No. DE-AC02-07CH11358. The Research at Oak Ridge National Laboratory's High Flux Isotope Reactor is sponsored by the Scientific User Facilities Division, Office of Basic Energy Sciences, U.S. Department of Energy. Use of the Advanced Photon Source at Argonne National Laboratory was supported by the U.S. Department of Energy, Office of Science, Office of Basic Energy Sciences, under Contract No. DE-AC02-06CH11357.

*hfli@ameslab.gov
†vaknin@ameslab.gov

[1] Y. Kamihara, T. Watanabe, M. Hirano, and H. Hosono, J. Am. Chem. Soc. **130**, 3296 (2008).
[2] X. H. Chen, T. Wu, G. Wu, R. H. Liu, H. Chen, and D. F. Fang, Nature (London) **453**, 761 (2008).
[3] Z. A. Ren, W. Lu, J. Yang, W. Yi, X. L. Shen, Z. C. Li, G. C. Che, X. L. Dong, L. L. Sun, F. Zhou, and Z. X. Zhao, Chin. Phys. Lett. **25**, 2215 (2008).
[4] A. D. Christianson, E. A. Goremychkin, R. Osborn, S. Rosenkranz, M. D. Lumsden, C. D. Malliakas, I. S. Todorov, H. Claus, D. Y. Chung, M. G. Kanatzidis, R. I. Bewley, and T. Guidi, Nature (London) **456**, 930 (2008).
[5] M. D. Lumsden, A. D. Christianson, D. Parshall, M. B. Stone, S. E. Nagler, G. J. MacDougall, H. A. Mook, K. Lokshin, T. Egami, D. L. Abernathy, E. A. Goremychkin, R. Osborn, M. A. McGuire, A. S. Sefat, R. Jin, B. C. Sales, and D. Mandrus, Phys. Rev. Lett. **102**, 107005 (2009).
[6] C. de la Cruz, Q. Huang, J. W. Lynn, J. Li, W. Ratcliff II, H. A. Mook, G. F. Chen, J. L. Luo, N. L. Wang, and P. Dai, Nature (London) **453**, 899 (2008).
[7] T. Nomura, S. W. Kim, Y. Kamihara, M. Hirano, P. V. Sushko, K. Kato, M. Takata, A. L. Shluger, and H. Hosono, Supercond. Sci. Technol. **21**, 125028 (2008).
[8] M. Ishikado, R. Kajimoto, S. Shamoto, M. Arai, A. Iyo, K. Miyazawa, P. M. Shirage, H. Kito, H. Eisaki, S. Kim, H. Hosono, T. Guidi, R. Bewley, and S. M. Bennington, J. Phys. Soc. Jpn. **78**, 043705 (2009).
[9] F.-J. Ma, Z.-Y. Lu, and T. Xiang, Phys. Rev. B **78**, 224517 (2008).
[10] S. Ishibashi and K. Terakura, J. Phys. Soc. Jpn. **77** (Suppl. C), 91 (2008).
[11] H.-F. Li, W. Tian, J. L. Zarestky, A. Kreyssig, N. Ni, S. L. Bud'ko, P. C. Canfield, A. I. Goldman, R. J. McQueeney, and D. Vaknin, Phys. Rev. B **80**, 054407 (2009).
[12] N. Qureshi, Y. Drees, J. Werner, S. Wurmehl, C. Hess, R. Klingeler, B. Buechner, M. Fernandez-Diaz, and M. Braden, arXiv:1002.4326 (unpublished).
[13] J. C. Loudon, C. J. Bowell, J. Gillett, S. E. Sebastian, and P. A. Midgley, Phys. Rev. B **81**, 214111 (2010).
[14] J.-Q. Yan, S. Nandi, J. L. Zarestky, W. Tian, A. Kreyssig, B. Jensen, A. Kracher, K. W. Dennis, R. J. McQueeney, A. I. Goldman, R. W. McCallum, and T. A. Lograsso, Appl. Phys. Lett. **95**, 222504 (2009).
[15] J. Rodríguez-Carvajal, Physica B **192**, 55 (1993).
[16] C. Fang, H. Yao, W. F. Tsai, J. P. Hu, and S. A. Kivelson, Phys. Rev. B **77**, 224509 (2008).
[17] H. Li, C. Broholm, D. Vaknin, R. Fernandes, D. Abernathy, M. Stone, D. Pratt, W. Tian, Y. Qiu, N. Ni, S. Diallo, J. Zarestky, S. Bud'ko, P. Canfield, and R. McQueeney, arXiv:1003.1687 (unpublished).
[18] A. Jesche, C. Krellner, M. de Souza, M. Lang, and C. Geibel, Phys. Rev. B **81**, 134525 (2010).
[19] Y. Xiao, Y. Su, M. Meven, R. Mittal, C. M. N. Kumar, T. Chatterji, S. Price, J. Persson, N. Kumar, S. K. Dhar, A. Thamizhavel, and Th. Brueckel, Phys. Rev. B **80**, 174424 (2009).
[20] P. J. Brown, *International Tables for Crystallography* (Kluwer Academic, Dordrecht, 1992).
[21] Y. Lee, D. Vaknin, H.-F. Li, W. Tian, J. L. Zarestky, N. Ni, S. L. Bud'ko, P. C. Canfield, R. J. McQueeney, and B. N. Harmon, Phys. Rev. B **81**, 060406(R) (2010).
[22] R. D. Shannon, Acta Crystallogr., Sect. A: Cryst. Phys., Diffr., Theor. Gen. Crystallogr. **32**, 751 (1976).
[23] T. Yildirim, Phys. Rev. Lett. **101**, 057010 (2008).
[24] I. Nowik, I. Felner, V. P. S. Awana, A. Vajpayee, and H. Kishan, J. Phys.: Condens. Matter **20**, 292201 (2008).
[25] J. Zhao, Q. Huang, C. D. L. Cruz, S. L. Li, J. W. Lynn, Y. Chen, M. A. Green, G. F. Chen, G. Li, Z. Li, J. L. Luo, N. L. Wang, and P. C. Dai, Nature Mater. **7**, 953 (2008).
[26] H.-F. Li, Y. Su, J. Persson, P. Meuffels, J. M. Walter, R. Skowronek, and Th. Brückel, J. Phys.: Condens. Matter **19**, 016003 (2007).
[27] H.-F. Li, Y. Su, J. Persson, P. Meuffels, J. M. Walter, R. Skowronek, and Th. Brückel, J. Phys.: Condens. Matter **19**, 176226 (2007).
[28] H.-F. Li, Y. Su, Y.-G. Xiao, J. Persson, P. Meuffels, and Th. Brückel, Eur. Phys. J. B **67**, 149 (2009).
[29] S. Mirbt, B. Sanyal, C. Isheden, and B. Johansson, Phys. Rev. B **67**, 155421 (2003).